Asynchronous Data Fusion for Vehicle Tracking Using MMW Radar and Magnetic Sensor in Tunnel

Guoqiang Mao*, Fellow, IEEE, Tianxuan Fu†, Xiaojiang Ren‡
* School of Transportation, Southeast University, Nanjing 211189, China
†Smart Transportation Institute and the School of Telecommunications Engineering, Xidian University, Xi'an 710071, China
‡ Smart Transportation Institute and the Guangzhou Research Institute, Xidian University, Xi'an 710071, China
futianxuan@stu.xidian.edu.cn

2025 IEEE Wireless Communications and Networking Conference (WCNC) | 979-8-3503-6836-9/25/$31.00 ©2025 IEEE | DOI: 10.1109/WCNC61545.2025.10978756

***Abstract*—Sensor fusion plays an increasingly important role in real-time traffic perception using roadside sensing devices because the use of single type of sensors often fail to deliver satisfactory performance in certain harsh environment. This paper investigates asynchronous data fusion for real-time vehicle tracking with inaccurate and randomly delayed measurements from millimeter-wave (MMW) radars and magnetic sensors in tunnel environment. We first propose a multisensor data association algorithm to assign the measurements of MMW radar and magnetic sensors to a particular vehicle. A tracking algorithm is then designed to asynchronously update the current vehicle states with randomly delayed magnetic sensor measurements. The proposed algorithm is implemented in the Xianfengding Tunnel, Jiangxi Province, China. Experiments validate the proposed method's accuracy using real data. The method and collected data form the basis of a real-time digital twin system to support advanced traffic management. The fusion results and measurement dataset are available at https://github.com/futianxuan/data.**

***Index Terms*—Asynchronous data fusion, roadside sensor, MMW radar, magnetic sensor, vehicle tracking.**

I. Introduction

Roadside traffic perception is crucial for developing a traffic digital twin system for advanced traffic management [1]. Continuous monitoring and transmission of traffic conditions to management centers facilitate smoother traffic movement and improve overall road safety.

Single-type sensors often produce incomplete and inaccurate data in harsh and dynamic environments. Cameras, the most commonly used roadside sensor, utilize AI-driven algorithms but face accuracy challenges due to poor lighting and occlusions [2]. LiDAR, while offering greater detection range and comprehensive data, requires high computing power and is affected by airborne particles [3]. MMW radar, a cost-effective alternative to LiDAR, is robust to environmental factors but has limited range and suffers from decreased accuracy at longer distances and in tunnels due to occlusion and multi-path interference [4].

Magnetic sensors have been extensively used for road traffic detection [5], [6]. Our previous works introduced smart studs—small, solar-powered, road-embedded Internet of Things (IoT) devices integrating magnetic sensors [7]. Magnetic sensors are robust to weather changes and unaffected by multi-path interference, complementing MMW radars, especially in tunnel environments. However, as the local magnetic field generated by a target attenuates quickly with propagation distance, magnetic sensors are generally only capable of lane-level detection and cannot detect targets too far away. The complementary nature of MMW radar and magnetic sensors, particularly in tunnel environments, motivates us to develop a robust detection system that fuses measurements from both magnetic sensor and MMW radar.

Multi-sensor fusion for asynchronous sensors is typically classified into centralized and distributed strategies. Centralized fusion, such as the centralized Kalman filter, is optimal but computationally expensive due to high-dimensional matrix operations. To mitigate this, a credibility measure combined with the KF [8] helps assess the validity of delayed measurements. Additionally, an adaptive Kalman filter (AKF) dynamically adjusts the Kalman gain based on sensor measurement quality, enhancing robustness to noise and model uncertainties [9]. In contrast, distributed fusion involves individual sensors generating local estimates, which are then combined by a fusion center to produce a globally optimal estimate, making it ideal when communication resources are limited. Asynchronous information fusion (AIF) for cameras and radar in intelligent driving systems has been addressed using matrix-weighted fusion algorithms for reliable estimates with a broad detection range [10], while a distributed covariance intersection (CI) fusion method has also been proposed for decentralized estimate fusion [11].

Timestamped data from heterogeneous sensors, such as MMW radar and magnetic sensors, are often asynchronous. While many methods assume uniform sampling intervals [12], this is unrealistic for systems with non-uniform sampling periods. Event-triggered systems execute tasks based on specific events, such as new measurements, leading to asynchronous sampling and estimation. In this paper, we address asynchronous data fusion involving aperiodic and delayed measurements that can impair vehicle tracking. To our knowledge, this is the first work considering delayed,

979-8-3503-6836-9/25/$31.00 ©2025 IEEE

aperiodic, and inaccurate measurements in asynchronous fusion of MMW radar and magnetic sensors for precise real-time vehicle tracking in a multi-lane tunnel scenario. The novelty and major contributions of this paper are summarized as follows:

1) To reduce computational complexity and the impact of false measurements, a data association algorithm is designed to match MMW radar and magnetic sensor measurements to vehicles using Hungarian and auction algorithms [13], respectively.
2) We present an asynchronous vehicle state update algorithm that updates the current state in one step using the randomly delayed measurements, unlike conventional methods requiring extensive historical data and iterative retrodiction.
3) The proposed heterogenous MMW radar and magnetic sensors based system is deployed in the Xianfengding Tunnel which allows validation of the accuracy and superiority of the proposed data fusion technique.

The rest of this article is organized as follows. Section II formulates the problem. Section III explains the proposed data association and real-time vehicle tracking algorithms. Section IV analyzes the performance of the algorithm and implementation in real tunnel scenarios. Section V presents the conclusions.

II. SYSTEM MODEL AND PROBLEM FORMULATION

The schematic diagram and deployment of MMW radars and magnetic sensors in a tunnel are illustrated in Fig. 1. The study considers a typical one-way and three-lane tunnel in China, but the proposed technique can be readily extended to tunnels with fewer or more lanes. Each lane has a width $L = 3.75\,m$. The lane boundary lines are numbered as $\{0, 1, 2, 3\}$, denoted by $\mathcal{O} = \{0, 1, 2, 3\}$, as shown in Fig. 1. The origin is defined as the center of the first magnetic sensor on the rightmost lane line in the driving direction. The x-axis aligns with the centerline of the rightmost lane boundary line, while the y-axis is locally perpendicular to the x-axis and points towards the leftmost lane. Here, a curvilinear coordinate system [14] is adopted, where the x-axis may be a curve. The curvilinear coordinate system helps to maximally utilize the knowledge that vehicles in most cases drive inside a lane, which can greatly simplify the estimation problem. The conversion from the curvilinear coordinate system to a global coordinate system can be readily done [15].

Magnetic sensors are positioned at equal intervals of L_a ($L_a = 15\,m$) along lane boundary lines 0 and 3 on both sides of the roadway. These sensors are denoted as $b_{0,j}$ and $b_{3,j}$ for the j-th sensors on lines 0 and 3, respectively. The middle lane boundary lines doe not magnetic sensors deployed because of the difficulty of supplying electricity to smart studs and the unavailability of solar energy in tunnel environments. MMW radars are installed at intervals of L_b ($L_b = 150\,m$) along the tunnel wall adjacent to Lane 1 at a height of 4.5 meters.

When a passing vehicle triggers magnetic sensors, measurement timestamps, lateral positions and lane line information are transmitted to the fusion center via LoRA, a low-rate wireless transmission method for IoT applications, at a non-periodic rate. In contrast, vehicle positions and speeds are periodically measured by MMW radars and transmitted to the fusion center via optical fibers due to the high data volume. Consequently, MMW radar and magnetic sensor data arrive at the fusion center with vastly different delays and loss rates. The fusion center conducts data association and vehicle state estimation using both data sources every T ($T = 0.1\,s$) seconds.

Given that the environment under consideration is a highway or a tunnel, a constant-velocity vehicle motion model is used to capture the kinematic relationship during tracking. Although more complex models like constant acceleration have been tested, they do not improve tracking accuracy. We focus on discrete time-varying linear systems evolving from time t_{k-1} to time t_k following a linear state space model:

$$x(k) = F(k, k-1)x(k-1) + \omega(k-1) \tag{1}$$

where the vehicle state is represented as $x(k) = [p_x(k), p_y(k), v_x(k), v_y(k)]^T$, $p_x(k)$ and $p_y(k)$ are the positions in portrait and lateral directions, respectively, $v_x(k)$ and $v_y(k)$ are the velocities. The system noise $\omega(k-1) = [w_x(k-1), w_y(k-1), w_{v_x}(k-1), w_{v_y}(k-1)]^T$ is a zero-mean white Gaussian noise with a known covariance matrix Q. $F(k, k-1)$ is the system transition matrix to t_k from t_{k-1}.

$$F(k, k-1) = \begin{bmatrix} 1 & 0 & \Delta t_k & 0 \\ 0 & 1 & 0 & \Delta t_k \\ 0 & 0 & 1 & 0 \\ 0 & 0 & 0 & 1 \end{bmatrix} \tag{2}$$

where $\Delta t_k = t_k - t_{k-1}$. Initial vehicle motion information is estimated separately from the MMW radars and magnetic sensors. The measurement equation of magnetic sensors and MMW radars is given by

$$z^i(k) = H^i(k)x(k) + v^i(k), \quad i \in \{r, b\} \tag{3}$$

where $z^r(k) = [z_{x,r}(k), z_{y,r}(k), z_{v_x,r}(k), z_{v_y,r}(k)]^T$ and $z^b(k) = [z_{x,b}(k)]$ are measurements of MMW radar and magnetic sensors, respectively, $z_{x,r}(k)$ and $z_{v_x,r}(k)$ are the lateral position and velocity obtained from MMW radar, while $z_{y,r}(k)$ and $z_{v_y,r}(k)$ correspond to the longitudinal position and velocity. Additionally, $z_{x,b}(k)$ indicates the x coordinate of the magnetic sensor. Parameter $H^i(k)$ is a known measurement matrix, $H^r(k) = \text{diag}[1, 1, 1, 1]$, $H^b(k) = [1, 0, 0, 0]$, and $v^i(k)$ is an additive zero-mean white Gaussian noise with a known covariance matrix $R^i(k)$. It is assumed that the MMW radar measurement noise and

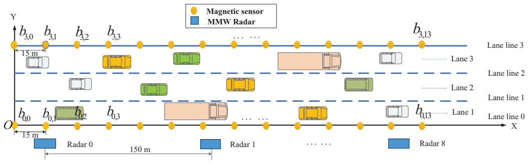

Fig. 1. A schematic diagram of the deployment of magnetic sensors and MMW radars in a three-lane tunnel.

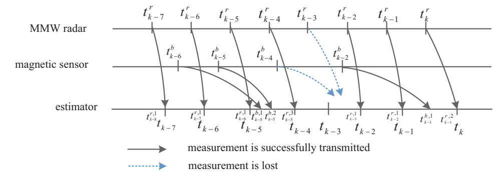

Fig. 2. An illustration of the estimation system with lost and delayed measurements. Parameter t_k represents the estimator time, t_k^r (t_k^b) is the MMW radar measurement (magnetic sensor measurement) time and $t_{k-1}^{r,1}(t_{k-1}^{b,2})$ is the time the MMW radar measurement (magnetic sensor measurement) is received at the estimator or the fusion center during $(t_{k-1}, t_k]$.

magnetic sensor noise are independent, and the measurement noise $v^i(k)$ is uncorrelated with the process noise $\omega(k)$.

Communication delay is almost inevitable in a networked environment and should be considered in the filter design. MMW radars are connected to a fiber-optic transmission system whereas magnetic sensors transmit their data through wireless and low datarate LoRA connections designed specifically for IoT applications. Therefore, transmission delays of magnetic sensors generally are much larger than MMW radar measurements. The MMW radar sampling time is set to be the same as the state update time. The time instant of the j-th measurement from sensor i, $i = \{r, b\}$, received at the fusion center during the interval $(t_k, t_{k+1}]$ are denoted as $t_k^{i,j}$, $j = 1, 2, ..., n$, and satisfy $t_k < t_k^{i,1} < t_k^{i,2} < \cdots < t_k^{i,n} \le t_{k+1} = t_k + T$. Due to aperiodic sampling and network-induced random delays, multiple measurements may be available, or no newly arrived measurement may occur during an estimation interval. Taking the estimation interval $(t_{k-1}, t_k]$ in Fig. 2 for example, where MMW radar measurement $z^r(t_k^r)$ and magnetic sensor measurement $z^b(t_{k-2}^b)$ are received during the state update interval $(t_{k-1}, t_k]$. Due to the very small transmission delays of MMW radar measurements, it is often the case that MMW radar measurements are generated and received during the same interval $(t_{k-1}, t_k]$ whereas magnetic sensor measurement $z^b(t_{k-2}^b)$ generated during $(t_{k-3}, t_{k-2}]$ is received a during a later interval, e.g., $(t_{k-1}, t_k]$. Due to the wireless low datarate LoRA connections being used, measurements from magnetic sensors often suffer from large delays and out-of-sequence arrivals at the fusion center as illustrated in Fig. 2. Therefore, the objective of this paper is to design an asynchronous data fusion method with time-varying delays and inaccurate measurements to achieve accurate vehicle tracking through advantageous combination of MMW radar and magnetic sensors.

III. Data Association and Real-Time Vehicle Tracking

As a vehicle approaches a tunnel entrance, it is first detected by an MMW radar. These radar measurements are associated with existing active tracks (data association details are outlined in Section III-A). Measurements that do not match existing tracks are used to initialize new targets, with their measurements establishing the states of these new targets and forming new tracks with unique IDs. The vehicle's motion is modeled as (1). Measurements from the MMW radars and magnetic sensors are then fed into the Kalman estimation process via (3). The state prediction is as follows:

$$x(k|k-1) = F(k,k-1)x(k-1) \tag{4}$$

$$P(k|k-1) = F(k,k-1)P(k-1)F(k,k-1)^T + Q(k-1) \tag{5}$$

where the state transition matrix $F(k, k-1)$ is provided in (2). The prediction module performs state predictions for all active tracks and synchronizes the states of all active tracks (or vehicles) to the same time t_k. This synchronized state is then used for the multisensor association and track update in the next step.

A. Measurement-Track Association

Considering the algorithm's complexity and limited computing resources, we design a low computational burden multisensor association algorithm using measurement-to-track association. Data association is divided into two steps: first, determining if the measurement falls within the association gate threshold; second, calculating the distance between the sensor measurements and the track's predicted measurement, then assigning the measurements to the tracks.

1) Data Association with MMW Radar: The Mahalanobis distance measures the distance between an MMW radar measurement and the state prediction by accounting for variable covariances and scale differences. This distance is particularly suitable as it normalizes the data and offers a consistent method to assess the similarity between observed measurements and predicted states. For an MMW radar measurement at time t_k, the square of the Mahalanobis distance between measurement m and the corresponding prediction of vehicle n is calculated as follows:

$$d_{mn}^2 = (z_m^r(k) - \hat{x}_n(k|k-1))^T S_{mn}(k)^{-1} (z_m^r(k) - \hat{x}_n(k|k-1)) \tag{6}$$

where $z_m^r(k)$ is the measurement vector of measurement m from MMW radar, and $\hat{x}_n(k|k-1)$ is the sate prediction vector of the vehicle n. The measurement covariance is $S_{mn}(k)$:

$$S_{mn}(k) = H^r(k)P_n(k|k-1)H^r(k)^T + R^r(k) \tag{7}$$

where $R^r(k)$ is the measurement noise covariance matrix and $P_n(k|k-1)$ is the covariance of the state prediction of vehicle n. The Mahalanobis distance values d_{mn} are recorded in the form of a matrix M_{dis}: the rows of the matrix M_{dis} are MMW radar measurements and the columns are the vehicles.

$$M_{dis} = \begin{cases} (d_{mn}^2)_{c\times l}, & if \ d_{mn}^2 \le G \\ d_{max}, & if \ d_{mn}^2 > G \end{cases} \tag{8}$$

Here, c is the number of sensor measurements, l denotes the number of tracks (or vehicles), and G is the association threshold. Only measurements within this threshold are considered for association. A large constant d_{max} indicates that a measurement is outside the track's threshold. Since the square of the Mahalanobis distance follows a chi-square distribution, with degrees of freedom based on the state vector's dimension, the threshold G is defined according to the chi-square distribution's probability table. For associating multiple measurements with vehicles, the Hungarian algorithm is employed due to its efficiency and effectiveness in solving the assignment problem. It ensures a globally optimal solution with polynomial time complexity, making it suitable for real-time applications. Measurements not associated are used to initialize new tracks, while successfully associated measurements update existing vehicle states.

2) Data Association with Magnetic Sensor: As discussed in Section II, a magnetic sensor measurement is triggered by a passing vehicle, recording the measurement timestamp and the location of the sensor. Assuming that after the estimation time epoch t_k, a magnetic sensor j generates a measurement with a timestamp t_j^b and the x coordinate denoted by x_j^b. Define $\sigma_{n,x}$ and $\sigma_{n,v}$as the standard deviations of the position and velocity estimates of vehicle n in the x direction, respectively. It follows that $\sigma_{n,x} = \sqrt{P_{k|k}(1,1)}$ and $\sigma_{n,v} = \sqrt{P_{k|k}(3,3)}$ where $P_{k|k}$ is the process covariance matrix of vehicle n at time t_k.

The estimated time for a vehicle n to arrive at the magnetic sensor j is

$$\hat{t}_{j,n} = t_k + \frac{x_j^b - \hat{p}_{x,n}}{\hat{v}_{x,n}} \tag{9}$$

where $\hat{p}_{x,n}$ and $\hat{v}_{x,n}$ are the estimated x coordinate and estimated speed along the x axis of vehicle n at time t_k, respectively. Without causing confusion and for ease of expression, we drop the subscript k from $\hat{p}_{x,n}$ and $\hat{v}_{x,n}$ and assume that the states of all active vehicles have been brought up to time t_k. Obviously, Equation (9) is an approximation only. Use $t_{j,n}$, $p_{x,n}$ and $v_{x,n}$ to denote the true values of $\hat{t}_{j,n}$, $\hat{p}_{x,n}$ and $\hat{v}_{x,n}$ respectively. It can be shown that

$$x_j^b = p_{x,n} + \frac{\int_{t_k}^{t_{j,n}} v_{x,n}(t)dt}{t_{j,n} - t_k}(t_{j.n} - t_k) = p_{x,n} + \bar{v}_{j,n}(t_{j,n} - t_k) \tag{10}$$

where $v_{x,n}(t)$ is the instantaneous speed at time t and $\bar{v}_{j,n} \triangleq \frac{\int_{t_k}^{t_{j,n}} v_{x,n}(t)dt}{t_{j,n}-t_k}$ is the time-averaged speed during $[t_k, t_{j,n})$. It follows from (10) that a more accurate approximation for $\hat{t}_{j,n}$ can be obtained from a first-order Taylor expansion:

$$\begin{aligned} \hat{t}_{j,n} &\approx t_k + \frac{x_j^b - \hat{p}_{x,n}}{\bar{v}_{j,n}} \\ &\approx t_k + \frac{x_j^b - \hat{p}_{x,n}}{\hat{v}_{x,n}} - \frac{x_j^b - \hat{p}_{x,n}}{(\hat{v}_{x,n})^2}\triangle v_{x,n} \end{aligned} \tag{11}$$

where $\triangle v_{x,n} = \bar{v}_{j,n} - \hat{v}_{x,n}$. It can be further shown that $Var\left(\frac{x_j^b - \hat{p}_{x,n}}{(\hat{v}_{x,n})^2}\triangle v_{x,n}\right) \approx \frac{(\sigma_{n,x})^2 + (\Delta x_{j,n})^2}{(\hat{v}_{x,n})^4}(\sigma_{n,v})^2$ where $\Delta x_{j,n} = x_j^b - \hat{p}_{x,n}$. Let

$$\sigma_{j,n} = \frac{\sqrt{(\sigma_{j,x})^2 + (\Delta x_{j,n})^2}}{(\hat{v}_{x,n})^2}\sigma_{n,v} \tag{12}$$

Based on the above analysis, we present the data association algorithm for magnetic sensor measurements. During the track initialization stage, the estimates of vehicle states may contain large errors. Therefore, it is more prudent to use the maximum and the minimum speed to form the association gate: $[t_k + \frac{\Delta x_{j,n}}{v_{max}} - \varepsilon_{t,j}, \hat{t}_j + \frac{\Delta x_{j,n}}{v_{min}} + \varepsilon_{t,j}]$, where v_{max} and v_{min} are respectively the maximum and the minimum speeds in a particular environment which can often be empirically determined, e.g., from the speed limit. The term $\varepsilon_{t,j}$ accounts for the difference between the local time of smart stud j and the true time. Due to synchronization error, the smart studs may have a time drift of up to $50\,ms$. When the vehicle state estimates have converged, a much reduced associate gate is used: $[t_k + \frac{\Delta x_{j,n}}{\hat{v}_{x,n}} - K_n\sigma_{j,n} - \varepsilon_{t,j}, t_k + \frac{\Delta x_{j,n}}{\hat{v}_{x,n}} + K_n\sigma_{j,n} + \varepsilon_{t,j}]$ where K_n is a value within $[2, 10]$ and is different for each vehicle. Parameter K_n is first assigned a larger value, e.g., 10. Each successful association with vehicle n allows us to reduce K_n a bit (normally by multiplying K_n by a constant smaller than 1, e.g., 0.9) till the minimum value of 2 is reached. If a vehicle n is unable to associate with any measurement, then K_n is multiplied by a constant larger than 1, e.g., 2, until the maximum value of 10 is reached. Such a procedure allows us to just filter in the "right" vehicles to associate with a particular measurement. If only one vehicle "falls" into the association threshold, that vehicle may be directly assigned to the measurement. However, it is often the case that multiple vehicles may be possibly associated with multiple measurements. In this case, the next step is invoked to resolve the optimum assignment.

For ease of expression, we use $t_{j,n,min}$ and $t_{j,n,max}$ to denote the aforementioned minimum and maximum association thresholds. Let t_j be the measurement timestamp from magnetic sensor j and $\tilde{t}_{j,n} = t_k + \frac{\Delta x_{j,n}}{\hat{v}_{x,n}}$ be the predicted time for vehicle n to arrive at sensor j using the state estimates of vehicle n. The gain of associating measurement from sensor j to vehicle n is given by:

$$\begin{aligned} a_{j,n} = & \frac{\max\left\{(t_j - t_{j,n,\min})^2, (t_j - t_{j,n,\max})^2\right\}}{\sigma_{j,n}} \\ & - \frac{(\tilde{t}_{j,n} - t_j)^2}{\sigma_{j,n}} \end{aligned} \tag{13}$$

The above gain optimally combines the distances from the association gate boundary and the distance between the predicted arrival time and the actual measurement timestamp, weighed by the uncertainty in vehicle state estimates captured by $\sigma_{j,n}$. The optimum data association problem can then be transformed into the maximization problem and solved using the auction algorithm [13]. Here, we used the auction algorithm for magnetic sensor measurements association due to its suitability for optimizing time-based cost differences in dynamic scenarios, where the focus is on efficiency and adaptability.

B. Vehicle State Update

After the data association problem is resolved, we then consider the update of the vehicle state in this subsection.

1) Sequential State Update with MMW radar measurements: After a new MMW radar measurement is associated with a track, the vehicle state estimate is performed sequentially, utilizing state prediction (4) and (5) and the subsequent state update as follows:

$$\begin{aligned} K(k) = & P(k|k-1)H^r(k)^T \\ & \times \left(H^r(k)P(k|k-1)H^r(k)^T + R^r(k)\right)^{-1} \end{aligned} \tag{14}$$

$$\hat{x}(k|k) = \hat{x}(k|k-1) + K(k)(z^r(k) - H^r(k)\hat{x}(k|k-1)) \tag{15}$$

$$P(k|k) = P(k|k-1) - K(k)H^r(k)P(k|k-1) \tag{16}$$

2) Out-of-Sequence Update of Randomly Delayed Magnetic Sensor Measurements: As previously mentioned, magnetic sensor measurements are transmitted to the fusion center via low data rate LoRa connections, which may cause significant delays, such as 1-2 seconds. In contrast, the transmission delays of MMW radar measurements are almost negligible, typically in the order of milliseconds. Consequently, it is common for a magnetic sensor measurement $z^b(\kappa)$ with a timestamp t_κ to arrive after the state has been updated at t_k, where $t_\kappa < t_k$. We can perform in one step the update with an l-step-lag delayed magnetic sensor measurements as follow:

The retrodiction of the state to t_κ from t_k is

$$\hat{x}(\kappa|k) = F(\kappa, k)\hat{x}(k|k) \tag{17}$$

The covariances associated with the state retrodiction are calculated as

$$P_{xv}(k, \kappa|k) = Q(k, \kappa) - P(k|k-l)S^*(k)^{-1}Q(k, \kappa) \tag{18}$$

where the covariance of the equivalent innovation at k in the Equation (18) can be expressed as:

$$S^*(k) = P(k|k-l) + R^*(k) \tag{19}$$

$$(R^*(k))^{-1} = (P(k|k))^{-1} - (P(k|k-l))^{-1} \tag{20}$$

Then the covariance matrix of state retrodiction can be calculated as

$$\begin{aligned} P(\kappa|k) = & F(\kappa, k)[P(k|k) + Q(k, \kappa) - P_{xv}(k, \kappa|k) \\ & - P_{xv}(k, \kappa|k)]^T F(\kappa, k)^T \end{aligned} \tag{21}$$

The covariance of the measurement for retrodicted state prediction is

$$S(\kappa) = H^b(\kappa)P(\kappa|k)\left(H^b(\kappa)\right)^T + R^b(\kappa) \tag{22}$$

The covariance between the estimated state at k and the delayed measurement is calculated as follows

$$P_{xz}(k, \kappa|k) = [P(k|k) - P_{xv}(k, \kappa|k)]\, F(\kappa, k)^T \left(H^b(\kappa)\right)^T \tag{23}$$

The filter gain used for the update is

$$K(k, \kappa) = P_{xz}(k, \kappa|k)S(\kappa)^{-1} \tag{24}$$

The update with the l-step-lag delayed magnetic sensor measurements $z^b(\kappa)$ of most recent state estimate $\hat{x}(k|k)$ is

$$\hat{x}(k|\kappa) = \hat{x}(k|k) + K(k, \kappa)[z^b(\kappa) - H^b(\kappa)\hat{x}(\kappa|k)] \tag{25}$$

The updated covariance at the current estimated time is

$$P(k|\kappa) = P(k|k) - P_{xz}(k, \kappa|k)S(\kappa)^{-1}[P_{xz}(k, \kappa|k)]^T \tag{26}$$

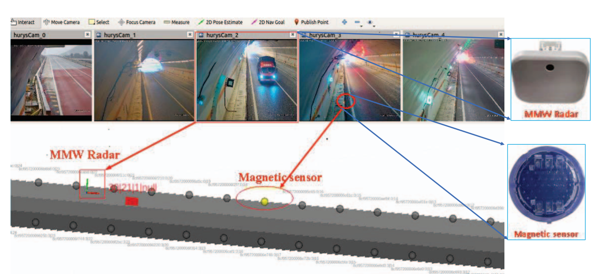

Fig. 3. The actual deployment plan and deployment photos of MMW radars and magnetic sensors in Xianfengding Tunnel, Jiangxi Province, China.

IV. Experimental Evaluation

A. Experimental Platform and Experiment Setup

The proposed system has been deployed in a commercial setting to form part of the advanced traffic and tunnel management system in Xianfengding Tunnel in Jiangxi Province, China, as shown in Fig 3. The three-lane tunnel, spanning approximately 1600 meters, is equipped with nine MMW radars and over 200 magnetic sensors to detect the real-time state of vehicles. The MMW radars are from Hurys Pty Ltd and with a model number DTAM D39-V. The initial covariance matrix is established as $P(0) = \text{diag}[0.01^2, 0.01^2, 0.05^2, 0.01^2]$. The covariance matrix of the MMW radar measurement noise is primarily determined by errors in transforming radar measurements from polar coordinates to Cartesian coordinates and is set to $R_r(0) = \text{diag}[0.5^2, 0.7^2, 0.05^2, 0.1^2]$. The covariance of the measurement noise from the magnetic sensor, considering the ranging error due to timing errors and the geomagnetic measurement error, is $R_b(0) = 25$, and the process noise covariance matrix is $Q_w(k) = \text{diag}[0.75T^2, 0.45T^2 1.5T, 0.9T]$.

B. Experimental Evaluation

In the actual deployment, it is difficult to obtain ground truth to gauge the accuracy of the state estimation. Following common practice in the field, we use the normalized innovation as a metric to measure the performance [16]. For example, when considering the horizontal position estimate, denoting the predicted state by $\hat{p}_{x,n}(k|k-1)$ and the measurement by $z_{x,n}(k)$ for a vehicle n, we calculate the normalized innovation of the n-th object over a time window with N_T measurements. It is defined as:

$$r_n = \frac{1}{N_T} \sum_k \left(\frac{(\hat{p}_{x,n}(k|k-1) - z_{x,n}(k))^2}{\sigma^2_{n,x}}\right) \tag{27}$$

This value represents the discrepancy between measurement and prediction. This metric is computed first for an object, and averaged in a certain time interval. The normalized innovation also employs the covariance matrices considering the predicted position uncertainties, $\sigma^2_{n,x}$ denote the variance of the prediction position of vehicle n in x direction, which has been given earlier.

The effectiveness of the proposed algorithm has been validated through experimental comparisons with state-of-the-art methods, as shown in Fig . 4. The KF exhibits higher median normalized innovation values in the x-direction, reflecting poor performance due to delayed measurements from the magnetic sensor. In contrast, the proposed algorithm shows lower maximum error values and more accurate, stable performance. In the y-direction, vehicle tracking faces higher uncertainty due to mis-detections from the magnetic sensor, which is influenced by vehicles in adjacent lanes. The bottom part of Fig. 4 highlights the significant reduction in normalized innovation and maximum error using the proposed method compared to others. The AIF performs sub-optimally, as its matrix-weighted fusion algorithm struggles with inaccurate measurements. The KF shows the highest median value but greater instability due to less accurate lateral measurements. Both CI and AKF exhibit similar median and maximum error values, indicating comparable performance. In contrast, the proposed method demonstrates the lowest normalized innovation and maximum error values, confirming its superior stability.

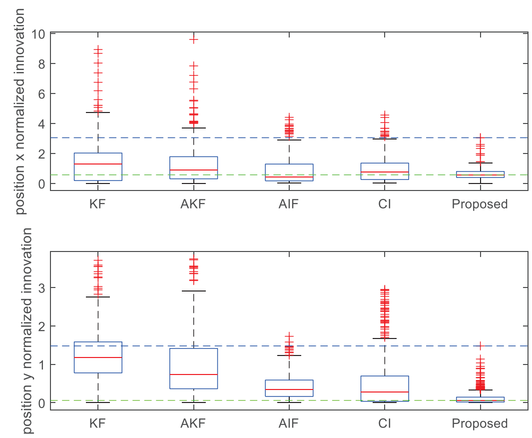

Fig. 4. Comparison of the position normalized innovation for x and y. Each box plot illustrates the distribution of the data. The box represents the interquartile range (IQR), which spans from the 25th percentile (lower quartile) to the 75th percentile (upper quartile), while the red line inside the box indicates the median value (50th percentile). The green and the blue dashed lines represent the median and maximum values of the proposed algorithm. It can be observed that the proposed algorithm exhibits the smallest maximum error values and minimum median values.

V. Conclusions

This work proposed a novel centralized asynchronous fusion method of MMW radars and magnetic sensors for real-time vehicle tracking. We studied the asynchronous estimation for discrete-time linear system with aperiodic state updating rate and nonuniform measurement sampling rate. A multisensor data association algorithm was designed to assign MMW radar and magnetic sensor measurements to specific vehicles. Additionally, the proposed fusion method was implemented in a real tunnel and helps to establish a traffic digital twin system for smart tunnel management. Experimental results demonstrated the effectiveness and cost-efficiency of the proposed method based on experiments conducted in Xianfengding Tunnel, Jiangxi, China. Future research will focus on addressing false or missed detection caused by sensors on either side being mistakenly triggered by vehicles in the middle lane and achieving precise lane-level vehicle tracking.

ACKNOWLEDGMENT

This work is supported by the National Natural Science Foundation of China under Grant U21A20446.

REFERENCES

[1] Guoqiang Mao, Yilong Hui, Xiaojiang Ren, Changle Li, and Yongjun Shao. The internet of things for smart roads: A road map from present to future road infrastructure. *IEEE Intelligent Transportation Systems Magazine*, 14(6):66–76, 2021.

[2] Ze Liu, Yingfeng Cai, Hai Wang, Long Chen, Hongbo Gao, Yunyi Jia, and Yicheng Li. Robust target recognition and tracking of self-driving cars with radar and camera information fusion under severe weather conditions. *IEEE Transactions on Intelligent Transportation Systems*, 23(7):6640–6653, 2021.

[3] Chenxi Tu, Eijiro Takeuchi, Alexander Carballo, Chiyomi Miyajima, and Kazuya Takeda. Motion analysis and performance improved method for 3d lidar sensor data compression. *IEEE Transactions on Intelligent Transportation Systems*, 22(1):243–256, 2019.

[4] Junpeng Shi, Guoping Hu, Xiaofei Zhang, and Fenggang Sun. Sparsity-based doa estimation of coherent and uncorrelated targets with flexible mimo radar. *IEEE Transactions on Vehicular Technology*, 68(6):5835–5848, 2019.

[5] Qing Wang, Jianying Zheng, Hao Xu, Bin Xu, and Rong Chen. Roadside magnetic sensor system for vehicle detection in urban environments. *IEEE Transactions on Intelligent Transportation Systems*, 19(5):1365–1374, 2017.

[6] Yimeng Feng, J Andrew Zhang, Bo Cheng, Xiangjian He, and Junliang Chen. Magnetic sensor-based multi-vehicle data association. *IEEE Sensors Journal*, 21(21):24709–24719, 2021.

[7] Yimeng Feng, Guoqiang Mao, Bo Chen, Changle Li, Yilong Hui, Zhigang Xu, and Junliang Chen. Magmonitor: Vehicle speed estimation and vehicle classification through a magnetic sensor. *IEEE Transactions on Intelligent Transportation Systems*, 23(2):1311–1322, 2020.

[8] Liping Yan, X. Rong Li, Yuanqing Xia, and Mengyin Fu. Modeling and estimation of asynchronous multirate multisensor system with unreliable measurements. *IEEE Transactions on Aerospace and Electronic Systems*, 51(3):2012–2026, 2015.

[9] Kai Shen, Yuelun Li, Tingxin Liu, Jianwen Zuo, and Ziao Yang. Adaptive-robust fusion strategy for autonomous navigation in gnss-challenged environments. *IEEE Internet of Things Journal*, 2023.

[10] Xiaohui Hao, Yuanqing Xia, Hongjiu Yang, and Zhiqiang Zuo. Asynchronous information fusion in intelligent driving systems for target tracking using cameras and radars. *IEEE Transactions on Industrial Electronics*, 70(3):2708–2717, 2022.

[11] Kunyang Cai, Ting Qu, Hong Chen, Bingzhao Gao, and Ning Bian. Low-cost hybrid multisensor fusion method and implementation for production intelligent vehicles. *IEEE Transactions on Instrumentation and Measurement*, 71:1–16, 2022.

[12] Yuxuan Shen, Zidong Wang, Hongli Dong, and Hongjian Liu. Multi-sensor multi-rate fusion estimation for networked systems: Advances and perspectives. *Information Fusion*, 82:19–27, 2022.

[13] Samuel S Blackman and Robert Popoli. Design and analysis of modern tracking systems. *(No Title)*, 1999.

[14] Junsoo Kim, Kichun Jo, Wontaek Lim, Minchul Lee, and Myoungho Sunwoo. Curvilinear-coordinate-based object and situation assessment for highly automated vehicles. *IEEE Transactions on Intelligent Transportation Systems*, 16(3):1559–1575, 2015.

[15] Kichun Jo, Minchul Lee, and Myoungho Sunwoo. Track fusion and behavioral reasoning for moving vehicles based on curvilinear coordinates of roadway geometries. *IEEE Transactions on Intelligent Transportation Systems*, 19(9):3068–3075, 2017.

[16] Jesús García, José Manuel Molina, and Jorge Trincado. Real evaluation for designing sensor fusion in uav platforms. *Information Fusion*, 63:136–152, 2020.